Validation of a Systematic Approach to Modeling Spray Quenching of Aluminum Alloy Extrusions, Composites, and Continuous Castings

D.D. Hall, I. Mudawar, R.E. Morgan, and S.L. Ehlers

Optimal cooling of aluminum alloys following the high-temperature extrusion process suppresses precipitation of intermetallic compounds and results in a part capable of possessing maximum strength and hardness after the subsequent age-hardening process. Rapid quenching suppresses precipitation but can lead to large spatial temperature gradients in complex-shaped parts, causing distortion, cracking, high residual stress, and/or nonuniform mechanical properties. Conversely, slow cooling significantly reduces or eliminates these undesirable conditions but allows considerable precipitation, resulting in low strength, soft spots, and/or low corrosion resistance. This study presents a systematic method of locating and operating multiple spray nozzles for any shaped extrusion such that uniform, rapid cooling and superior mechanical and metallurgical properties are achieved. A spray nozzle data base was compiled by measuring the distribution of spray hydrodynamic parameters (volumetric spray flux, mean drop diameter, and mean drop velocity) throughout the spray field of various industrial nozzles. Spray heat transfer correlations, which link the local spray hydrodynamic parameters to the heat transfer rate in each of the boiling regimes experienced by the surface, defined the spatially nonuniform boundary conditions in a numerical model of the quenching process that also accounted for interference between adjacent spray fields. New correlations, offering increased accuracy and less computational time, were formulated for the high-temperature boiling regimes which have a critical influence on final mechanical properties. The quench factor technique related predicted thermal history to metallurgical transformations occurring within the extrusion to predict hardness distribution. The validity of this unique approach was demonstrated by comparing model predictions to the temperature response (and hardness after artificial aging) of an L-shaped Al 2024-T6 extrusion to quenches with multiple, overlapping water sprays. The validation study reported herein concludes by exploring the possibility of applying quenching technology to improving the properties of extruded metal-matrix composites such as SiC_p/Al 6061 and cast alloys.

Keywords

aluminum alloys, computer model, quenching, spray quenching

1. Introduction

ALUMINUM alloys are used for a wide range of applications, from common household products such as storm-screen window frames to structural members in military and commercial aircraft. Aluminum has been used extensively in the aerospace industry for its high strength-to-weight ratio and corrosion resistance. Recently, these same attributes, coupled with the promise of full recyclability, have made aluminum a possible substitute for steel in automobile components, including frame, body panels, and engine block. In fact, production of the so-called aluminum-intensive vehicle (AIV) is already underway in Europe; U.S. automakers plan to introduce their own AIV within a few years. Lightweight aluminum components may also compensate for the relatively low power of electric vehicles. The success of these vehicles is expected to be heavily dependent upon the automaker's ability to both reduce cost and develop innovative aluminum processing techniques.

D.D. Hall and **I. Mudawar,** Boiling and Two-Phase Flow Laboratory, School of Mechanical Engineering, Purdue University, West Lafayette, IN 47907-1288, USA; and **R.E. Morgan** and **S.L. Ehlers,** Naval Air Warfare Center, Aircraft Division—Indianapolis, Indianapolis, IN 46219-2189, USA.

The aluminum industry is presently in dire need of systematic, cost-effective methods for fabrication of complex-shaped, high-strength aluminum alloy parts. Heat treatment is a prime example of a fabrication process where poor technical know-how and the absence of a systematic production method have contributed to both poor quality and high production costs. In fact, it is well known throughout the aluminum industry that a large fraction of the cost of producing aluminum parts is associated with post-treatment operations involving additional heat treatment and mechanical straightening of warped sections.

Heat treatment of aluminum alloys is a three step process:

1. *Solution heat treatment:* heating the part to a temperature near but below the melting point and holding for a time long enough such that the alloying elements diffuse into the aluminum grain structure, forming a nearly homogeneous solid solution
2. *Quenching:* rapidly cooling the part from the solution heat treatment temperature in order to suppress solute precipitation and virtually "freeze" the supersaturated solid solution (slow cooling produces massive precipitation along the aluminum grain boundaries resulting in a microstructure that cannot be enhanced by the aging process)
3. *Artificial aging:* reheating the part to some intermediate temperature for a specified duration (while avoiding over-aging) in order to form a fine dispersion of precipitates within the aluminum grains, leading to a substantial hard-

Nomenclature

c_p	specific heat at constant pressure	Pr	Prandtl number
C_t	critical time defined in Eq 1 and Fig. 2	q''	heat flux
d_{32}	Sauter mean diameter (SMD)	Q''	volumetric spray flux
h	convection heat transfer coefficient	R	universal gas constant, 8.314 J gmol^{-1} K^{-1}
h_{fg}	latent heat of vaporization	Re_{32}	Reynolds number, $\rho_f Q'' d_{32}/\mu_f$
H	Rockwell B hardness	t	time
k	thermal conductivity	T	temperature
k_1	natural logarithm of hardness ratio (or fraction of solute not precipitated) used to define the C-curve	ΔT	$T_s - T_f$
		ΔT_{sub}	liquid subcooling, $T_{sat} - T_f$
k_j	empirical constant in the C-curve equation, $j = 2, 3, 4$, or 5	U_m	mean drop velocity
		x	coordinate along spray major axis
Nu_{32}	Nusselt number, $h\, d_{32}/k_f$	y	coordinate along spray minor axis

Greek symbols

μ	dynamic viscosity	σ	yield strength; surface tension
ρ	density	τ	quench factor

Subscripts

CHF	critical heat flux	min	minimum
DFB	departure from film boiling	MHF	minimum heat flux
f	saturated liquid, final condition	OSP	onset of single-phase cooling
g	saturated vapor	s	surface condition
i	initial condition	sat	saturated condition
max	maximum		

ening of the alloy (precipitates act as dislocation barriers since they impede deformation of the part when it is later subjected to stress)

Quenching is the most critical stage of heat treatment. From a microstructural point of view, it is desirable to cool the entire part as quickly as possible from the solution heat treatment temperature. However, most extrusions possess cross sections with large variations in thickness, causing thinner sections to cool much faster than the interior of thick sections. Large temperature gradients may exist during the quench, leading to large thermal stresses and, hence, residual stresses and possible warping or cracking. An inferior quench remains by far the greatest source of imperfections in aluminum alloys, including, aside from the aforementioned residual stresses, low corrosion resistance and soft spots. All of these imperfections are known to lead to low strength and premature part failure.

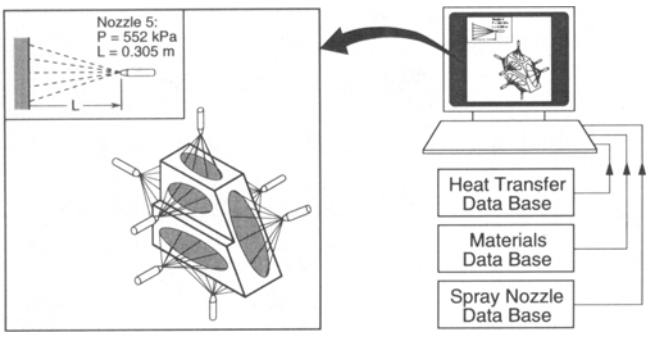

Fig. 1 CAD/CAM intelligent spray quenching system

Spray quenching has recently emerged as the quenching method of choice, since, unlike bath quenching (submerging the part in a liquid bath), the part can be cooled by arrays of individually configured high-pressure water sprays upon exiting the extrusion die. Spray cooling allows the local surface heat flux (i.e., cooling rate) to be controlled, whereas bath quenching offers no control, since the entire part is constantly in contact with the coolant. Denser sprays can therefore be aimed at the thicker sections and lighter sprays at the thinner ones. An ideal quench consists of both rapid and uniform cooling of the part. Although spray quenching offers a workable solution to the process of heat treating, an infinite number of possible spray configurations exist, and no method exists in the aluminum industry for optimizing the type, location, and flow rate of the sprays to produce the desired quench. Presently, configuring an acceptable spray quenching system is a very costly venture that is based, especially for small-batch heat treatment operations, on the visual appearance of the part and the experience of the operator. The spray configuration is modified by trial and error until post-heat-treatment tests reveal that acceptable properties were obtained. Unfortunately, an optimum configuration can seldom be determined with certainty.

The present study is the focus of a cross-disciplinary endeavor at the Purdue University Boiling and Two-Phase Flow Laboratory, whose primary goal is the development of the CAD/CAM intelligent spray quenching system proposed by Deiters and Mudawar (Ref 1) and illustrated in Fig. 1. The operator of the heat treating facility would simply enter the alloy

composition and part geometry into the CAD/CAM system. Upon consulting its extensive data bases, the system would determine the nozzle configuration (type, placement, and pressure) required to achieve optimum cooling and produce parts having superior mechanical and metallurgical properties, thus eliminating the costly trial and error procedure utilized today in industry. This study summarizes the important aspects of the intelligent spray quenching system, including recent developments by the authors in regard to predicting the thermal history and hardness distribution of heat-treated extrusions. Also, new and improved spray heat transfer correlations are presented for modeling the thermal boundary condition of a spray-quenched metallic part. The manuscript concludes by exploring the possibility of applying quenching technology to improving the properties of extruded metal-matrix composites and cast alloys.

2. Relationship between Local Quench Rate and Strength of Heat-Treated Alloys

The present study deals with the 2*xxx* series of wrought aluminum-copper alloys, specifically Al 2024 (93.5% Al, 4.4% Cu, 1.5% Mg, 0.6% Mn), which are characterized by their ability to be significantly strengthened by artificial aging (precipitation hardening). Fink and Willey (Ref 2) pioneered the attempt to describe the relationship between cooling rate (quenching rate) and final alloy strength by identifying the temperature range over which the cooling rate has its most critical influence on the mechanical properties of the aged material. Their research resulted in the development of the C-curve, which represents the critical time required at different temperatures to precipitate a sufficient amount of solute (alloying elements) to reduce the maximum attainable strength or hardness by the percentage represented by that particular C-curve. Figure 2 shows the C-curve representing 99.5% of the maximum attainable hardness for Al 2024-T6 (Ref 3). If a small Al 2024 sample was rapidly quenched from the solution heat treatment temperature to an intermediate temperature, held for the critical time, rapidly quenched to room temperature, and artificially aged to achieve the T6 temper, then the resulting hardness would be 99.5% of the hardness attained if the sample were instantaneously quenched from the solution heat treatment temperature to room temperature. Fink and Willey (Ref 2) used the average quenching rate through the temperature range where the precipitation rate is highest (indicated by the shaded region in Fig. 2) to assess the quality of a quenching process. However, when cooling rates vary considerable during the quench (e.g., in a complex-shaped part), quantitative predictions of the final material properties using average quenching rates are not possible.

The quench factor technique developed by Evancho and Staley (Ref 4, 5) couples the time required for precipitation of the solute (i.e., C-curve) with the time available for precipitation (i.e., temperature-time cooling history of the quenched part) to predict the effect of quenching on the final mechanical properties of wrought alloys. Cahn (Ref 6) showed that a relative measure of the amount of precipitation during a continuous cooling process is given by:

$$\tau = \int_{t_i}^{t_f} \frac{dt}{C_t} = \sum_{m=1}^{n} \frac{\Delta t_m}{C_{t,m}} \qquad \text{(Eq 1)}$$

where τ was later referred to as the quench factor (Ref 4). Quench factors of zero and infinity correspond to suppression of precipitation and complete precipitation, respectively. The integral in Eq 1 can be calculated by discretizing the temperature-time curve into a series of small time increments (i.e., approximating an actual quench as a series of isothermal quenches), thus allowing a transient cooling process to be studied using isothermal precipitation kinetics. Each incremental quench factor represents the ratio of the amount of time the alloy was at a certain temperature to the amount of time required to obtain a specified amount of solute precipitation at that temperature.

Since the hardness of age-hardenable aluminum alloys is proportional to strength (Ref 7, 8) and because the relative strength of age-hardenable aluminum alloys is directly related to the amount of solute (alloying elements) remaining in solid solution after the quench (Ref 9), Evancho and Staley (Ref 4, 5) utilized isothermal precipitation kinetics to show that:

$$\frac{H - H_{min}}{H_{max} - H_{min}} = \frac{\sigma - \sigma_{min}}{\sigma_{max} - \sigma_{min}} = \exp(k_1 \tau) \qquad \text{(Eq 2)}$$

where σ_{max} (or H_{max}) and σ_{min} (or H_{min}) are the maximum and minimum yield strength (or hardness) of age-hardened speci-

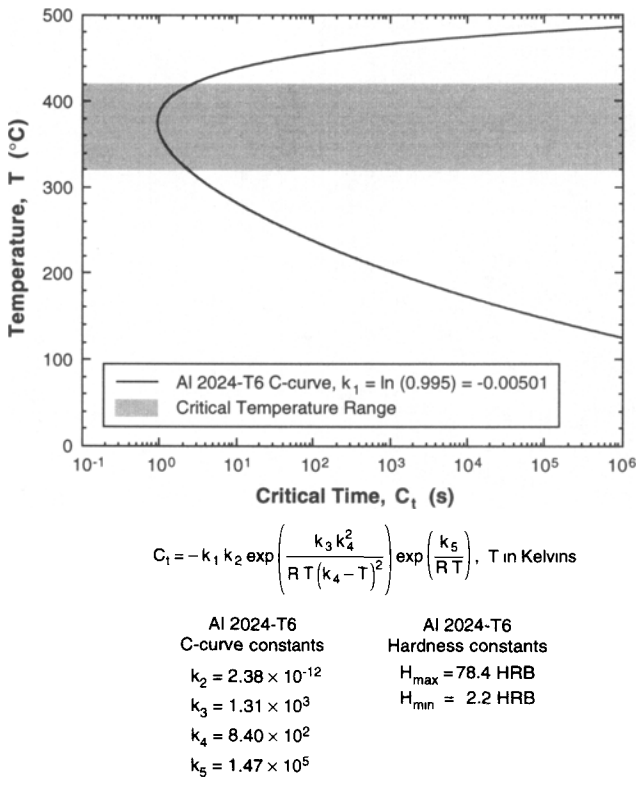

Fig. 2 C-curve representing 99.5% of the maximum attainable hardness for Al 2024-T6. Source: Ref 3

mens which have been cooled from the solution heat treatment temperature at a near infinite and extremely slow rate, respectively. Note that k_1 in Eq 2 is the natural logarithm of the hardness (or strength) ratio corresponding to the C-curve from which the quench factor was calculated. Thus, given the thermal history and C-curve of an alloy, the final mechanical properties (strength or hardness) of the part can be determined using the quench factor technique. Prior to the present study, the quench factor technique had only been successfully used to predict the yield strength and hardness of *small* (i.e., isothermal at any instant during the quench) aluminum alloy parts (Ref 3, 4, 10-13) and steel parts (Ref 14, 15) subjected to *bath quenching*.

3. Spray Heat Transfer

The quenching of aluminum and other metallic alloys is initiated at high temperatures well above the saturation temperature of the liquid coolant. Figures 3(a) and (b) show a boiling curve and a temperature-time curve (cooling curve, quench curve), respectively, illustrating the several distinct heat transfer regimes experienced by a quenched surface. Initially, the surface encounters the film boiling regime, which is characterized by the formation of an insulating vapor blanket between the surface and impinging droplets, resulting in poor heat transfer. Intermittent wetting and reformation of the vapor blanket, which occurs between the point of departure from film boiling (DFB) and the point of minimum heat flux (MHF), was labeled as a film wetting regime by Klinzing et al. (Ref 16). As the temperature decreases below MHF, the vapor blanket begins to collapse, and permanent, partial wetting of the surface occurs. This transition boiling regime is marked by a significant increase in the surface heat flux due to local areas of intense boiling, thus causing a rapid decrease in surface temperature. The vapor layer virtually vanishes at the point of critical heat flux (CHF), and cooling rates remain fairly high in the ensuing nucleate boiling regime as the entire surface experiences liquid contact. Boiling completely subsides in the single-phase cooling regime, and heat transfer is simply due to forced convection with the impinging liquid.

3.1 Spray Hydrodynamic Parameters

Mudawar and Valentine (Ref 17) demonstrated that heat transfer to water sprays depends solely upon the local values of the spray hydrodynamic parameters (volumetric spray flux, mean drop diameter, and mean drop velocity) just prior to impingement upon the surface. Volumetric spray flux, Q'', is defined as the local volume flow rate per unit surface area. The Sauter mean diameter, d_{32}, is the diameter of a spherical drop whose ratio of volume to surface area is the same as that of the entire measurement sample. Mean drop velocity, U_m, is simply the average of measured individual drop velocities. Volumetric spray flux distributions were well represented by a curve-fit which exhibited a maximum value near the center of the spray and decayed exponentially away from the center (Ref 18). Sauter mean diameter and mean drop velocity did not vary significantly within a spray. Table 1 summarizes the spatial distribution models of the spray hydrodynamic parameters for nozzles used in this study (see Ref 18 for additional details).

3.2 Heat Transfer Correlations

A series of studies on heat transfer from hot metallic surfaces to industrial sprays commonly employed in materials processing was performed at the Purdue University Boiling and

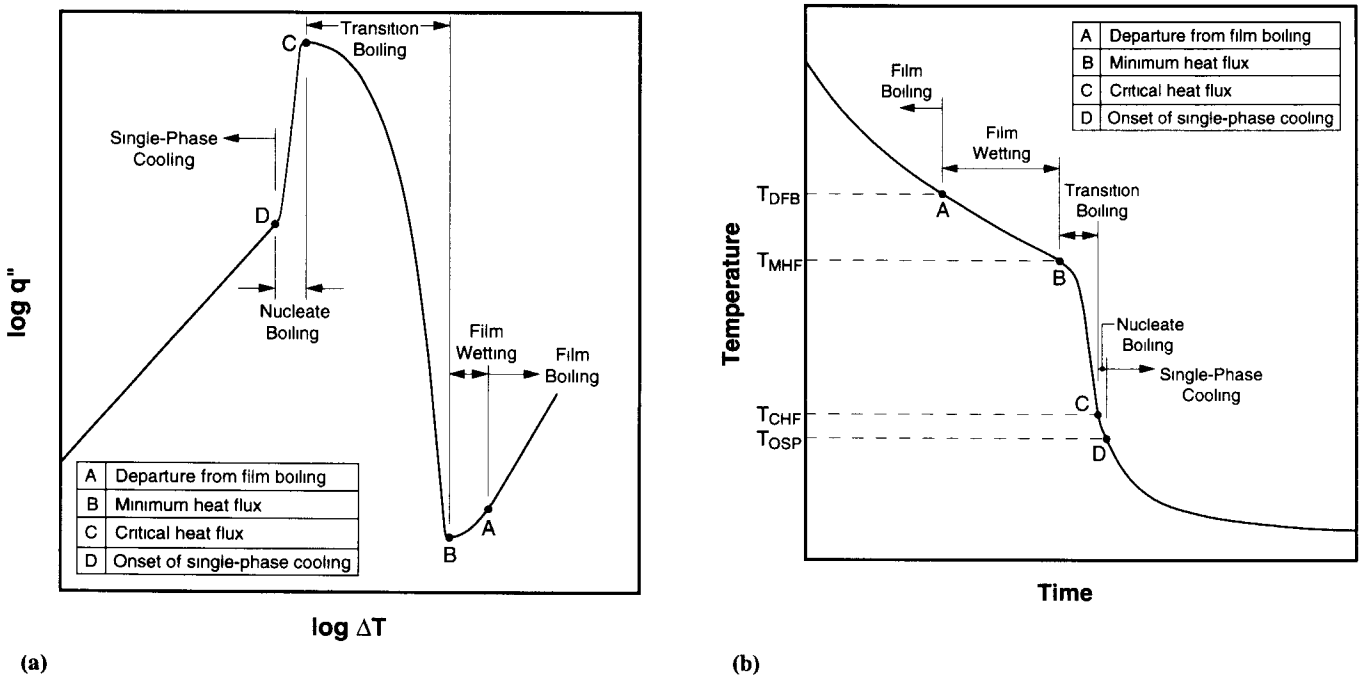

Fig. 3 (a) Boiling curve and (b) thermal response of a quenched surface, showing the four temperatures at which the surface enters a new boiling regime and requires a different correlation to determine the heat transfer coefficient

Two-Phase Flow Laboratory (Ref 16, 17). Several stainless steel full cone and flat spray nozzles were operated at various nozzle-to-surface distances and pressures to obtain a wide range of the spray hydrodynamic parameters. Mudawar and Valentine (Ref 17) utilized a steady-state measurement technique to measure local heat transfer rates within a spray field. Heat was supplied to an insulated calorimeter bar which had its exposed surface positioned at the center of the downward impinging spray. The small cross-sectional area of the calorimeter bar (0.5 cm^2) allowed the detection of sharp spatial gradients in the heat transfer coefficient within the spray field. The heat flux at steady state was determined from the uniform temperature gradient between thermocouples placed along the axis of the calorimeter bar. The linear temperature distribution was extrapolated to the surface to obtain the steady-state surface temperature. Input power was increased in small increments so that a nearly continuous boiling curve was obtained upon processing of the data. Heat transfer correlations (see Table 2) based on surface temperature, fluid properties, and the local spray hydrodynamic parameters were developed for the nucleate boiling and single-phase cooling regimes, as well as CHF and incipient boiling (onset of single-phase cooling or OSP). Mudawar and Deiters (Ref 19, 20) later concluded that these correlations, which were developed from measurements at the geometric center of the sprays, were valid at other locations within the spray field when the spray hydrodynamic parameters were determined for these locations. The transition to film boiling was unsteady, so an alternate method was required to characterize these high-temperature boiling regimes.

Klinzing et al. (Ref 16) developed a technique for extracting the surface heat flux from the transient temperature history of a quenched disk. Using the lumped capacitance method, disk temperature was assumed to be uniform at every instant during the quench. From the measured temperature response, the instantaneous surface heat flux was determined by solving the transient heat diffusion equation for a lumped mass. Correlations for the film boiling regime, DFB, and MHF were formulated from these boiling curves. The heat flux correlations for the film wetting and transition boiling regimes were chosen to be polynomial functions of ΔT. The unknown constants were determined by forcing the curve-fits to yield a maximum heat flux at CHF and a minimum at MHF. Furthermore, continuity of heat flux was required at the transitions between boiling regimes. The nucleate boiling and single-phase cooling regimes could not be characterized using the transient measurement technique, since the relatively high heat transfer coefficient violated the lumped mass approximation.

3.3 Previous Modeling of Spray Quenching

Mudawar and Deiters (Ref 19, 20) accurately predicted the temperature history (below about 200 °C) of an Al 1100 block which was sprayed over one surface and whose other surfaces were well insulated. Kim et al. (Ref 3) and Wang et al. (Ref 21) ignored the spatial variation of spray hydrodynamic parameters and incorrectly used a single boiling curve to determine the boundary heat flux at all surface locations being sprayed. Furthermore, Kim et al. and Wang et al. assumed that the entire surface was uniformly sprayed and presented no experimental validation of their numerical models. Zabaras et al. (Ref 22) utilized the nonlinear inverse heat conduction method to obtain the transient thermal boundary condition from temperatures measured within a cylindrical extrusion quenched in an agitated water bath. This costly and time-consuming method depends on part geometry and cannot be accomplished without experimental data for each new part to be produced. The above studies offer only limited insight into the simulation and optimization of an industrial spray quenching process.

Flat spray nozzles are commonly used in industrial quenching operations because their elliptical spray pattern can provide relatively even spray coverage when several nozzles with overlapping spray patterns are utilized. Typically, the quenching phase of a heat treatment operation consists of either a stationary part or a long extrusion moving through an array of overlapping sprays. Klinzing et al. (Ref 16) and Rozzi et al. (Ref 23) were the first researchers to utilize heat transfer correlations independent of part geometry to predict the two-dimensional thermal response of a part quenched with flat sprays in a simulated industrial environment. Klinzing et al. attained limited success with the quenching of a thin, rectangular Al 1100 plate; Rozzi et al. significantly overpredicted the heat transfer rate of a quenched L-shaped extrusion because, in the opinion of the present authors, their nozzle configuration permitted a large axial variation of the heat transfer coefficient, causing the problem to become three-dimensional.

The present study aims to eliminate the deficiencies of these earlier attempts at modeling the spray quenching of metallic alloys. Obviously, the most critical aspects of any model are the spray quenching heat transfer correlations and the spray interaction model. Spray interaction between adjacent nozzles whose major axes coincide was investigated, and a methodology was developed for optimizing nozzle spacing and adapting single-nozzle models for use with nozzle arrays having overlapping spray patterns (see Ref 18 for additional details). The nozzle configuration used in the present study eliminates the

Table 1 Spatial distribution models of the spray hydrodynamic parameters for several spray nozzles

Nozzle type (spray angle)	Fluid (temperature)	Pressure, kPa (psig)	Distance, m (in.)	Flow rate, $m^3 s^{-1} \times 10^6$ (gpm)	$d_{32} \times 10^6$, m	U_m, m s^{-1}	$Q''(x,y)$ (a), $m^3 s^{-1} m^{-2}$
Full cone (48°)	Water (23 °C)	276 (40)	0.381 (15.0)	42 (0.67)	544	18.7	1.04×10^{-3}(b)
Full cone (27°)	Water (23 °C)	138 (20)	0.483 (19.0)	132 (2 1)	1160	16.5	5.06×10^{-3}(b)
Full cone (51°)	Water (23 °C)	552 (80)	0.305 (12.0)	18 (0.28)	286	13.5	$4.24 \times 10^{-3} \exp(-143\,x^2 - 3790\,y^2)$

(a) The coordinates x and y, shown in the $Q''(x, y)$ equation, have units of meters. (b) Insufficient measurements to develop a spatial distribution model of the volumetric spray flux. The value shown is the volumetric spray flux directly beneath the nozzle orifice at the distance specified.

undesired longitudinal nonuniformity in the heat transfer coefficient and the majority of axial temperature gradients in a stationary testpiece and permits the quenching process to be analyzed using a two-dimensional numerical model. The present study focuses on the spray quenching heat transfer correlations developed by Klinzing et al. and Rozzi et al. and recommends significant improvements which increase accuracy and decrease computational time.

3.4 *Improved Spray Heat Transfer Correlations*

Boiling curves for various sprays were constructed from the heat transfer correlations developed by Mudawar et al. resulting in the discovery of a discontinuity in the boiling curve at DFB, lower heat fluxes in the film boiling regime than at MHF, and an unrealistic description of the film wetting regime. New correlations for DFB, MHF, and the film wetting regime were formulated by the present authors to ensure that the set of correlations produces a smooth, continuous boiling curve that observes the correct trends for all possible combinations of the spray hydrodynamic parameters.

The DFB heat flux correlation always predicted a higher heat flux than the film boiling correlation evaluated at ΔT_{DFB}, causing an abrupt increase in heat flux as temperature decreased (i.e., the boiling curve was overconstrained at DFB). Either the DFB heat flux correlation or the DFB temperature correlation must be reformulated using the film boiling correlation in order to have continuity at DFB. A new DFB temperature correlation was derived by equating the DFB heat flux correlation (Ref 16) to the film boiling heat flux correlation (Ref 16) and solving for ΔT. Since the unaltered DFB heat flux correlation always yielded a higher heat flux than the MHF heat flux correlation, this new DFB temperature correlation ensured that MHF remained a local minimum in the boiling curve. If, instead, a new DFB heat flux correlation had been derived by substituting the DFB temperature correlation into the film boiling heat flux correlation, this would have incorrectly allowed lower heat fluxes at DFB than at MHF.

The previous film wetting heat flux correlation (Ref 16) was a quadratic equation in ΔT, with the constants determined by requiring the heat fluxes at the regime boundaries (determined by the DFB and MHF temperature correlations) to be equal to that predicted by the DFB and MHF heat flux correlations. The correlation also required a zero slope in the boiling curve at MHF; however, the slopes in the film wetting and film boiling regimes were not matched at DFB. A new correlation for the heat flux in the film wetting regime was proposed by assuming a cubic equation:

$$q'' = C_0 + C_1\Delta T + C_2\Delta T^2 + C_3\Delta T^3 \quad \text{(Eq 3)}$$

In this case, the coefficients were determined by requiring the boiling curve to be both continuous and smooth (differentiable) at DFB and MHF. In other words, at DFB ($\Delta T = \Delta T_{DFB}$):

$$q'' = q''_{DFB} \quad \text{(Eq 4a)}$$

$$\frac{\partial q''}{\partial \Delta T} = \left.\frac{\partial q''_{\text{film boiling}}}{\partial \Delta T}\right|_{DFB} \quad \text{(Eq 4b)}$$

and at MHF ($\Delta T = \Delta T_{MHF}$):

$$q'' = q''_{MHF} \quad \text{(Eq 5a)}$$

$$\frac{\partial q''}{\partial \Delta T} = \left.\frac{\partial q''_{\text{transition boiling}}}{\partial \Delta T}\right|_{MHF} = 0 \quad \text{(Eq 5b)}$$

The new film wetting correlation is given in Table 2.

The reformulation of the DFB temperature correlation created the possibility of a DFB temperature lower than the MHF temperature or a boiling curve with a steeper slope in the film wetting regime than in the film boiling regime; both of which occur at relatively low volumetric spray flux. If either of these conditions existed for a particular combination of spray hydrodynamic parameters, then the film wetting regime was assumed to be absent. In this case, film boiling persisted until the occurrence of MHF as defined by the MHF temperature correlation; the MHF heat flux correlation was replaced with the film boiling correlation evaluated at ΔT_{MHF}. Physically, this phenomenon can be interpreted as a lack of liquid impinging and disrupting the vapor layer on the surface, permitting a stable vapor layer until the transition boiling regime.

3.5 *Validation of the Heat Transfer Correlations*

Figure 4 shows the excellent agreement between transient (above CHF) and steady-state (below CHF) heat transfer data obtained at the center of two different full cone sprays with boiling curves generated from the heat transfer correlations and local spray hydrodynamic parameters. Because of the invariance of mean drop velocity and diameter within a spray field, the volumetric spray flux has a dominant effect on heat transfer, except in the nucleate boiling regime, which is insensitive to the spray hydrodynamic parameters. Figures 5(a) and (b) display models of the two-dimensional volumetric spray flux distribution for a single flat spray and the optimized nozzle configuration utilized in the present study (three flat spray nozzles separated by 11.4 cm (4.5 in.), along the axis of the nozzle array), respectively. Figure 5(c) shows predicted boiling curves for volumetric spray fluxes corresponding to the contour lines in Fig. 5(a) and (b). The slope of the boiling curve in both the single-phase cooling regime and the film boiling regime is unaffected by volumetric spray flux. Heat fluxes at OSP vary by an order of magnitude, while CHF, MHF, and DFB vary somewhat less. As spray flux decreases, the gradual change in slope characteristic of the film wetting regime becomes less noticeable and finally disappears at approximately 1.0×10^{-3} m^3 s^{-1} m^2. Figure 5 also reveals that heat transfer rates will vary drastically within a short distance along a quenched surface due to the variation of volumetric spray flux. In addition, Fig. 5(a) and (b) illustrate the importance of optimizing the nozzle configuration so that neither the volumetric spray flux nor the heat transfer coefficient varies in the axial direction.

Table 2 Spray quenching heat transfer correlations

Quenching (Boiling) Regime	Correlation
Film Boiling Regime (Ref 16)	$q'' = 63.25\,\Delta T^{1.691}\,Q''^{0.264}\,d_{32}^{-0.062}$
Point of Departure from Film Boiling	$\Delta T_{DFB} = 886.2\,Q''^{0.192}\,U_m^{0.144}\,d_{32}^{0.0367}$ $q''_{DFB} = q''_{\text{film boiling}}\big\vert_{DFB} = 63.25\,\Delta T_{DFB}^{1.691}\,Q''^{0.264}\,d_{32}^{-0.062}$ $= 6.100\times10^{6}\,Q''^{0.589}\,U_m^{0.244}$
Film Wetting Regime	If $\Delta T_{DFB} \le \Delta T_{MHF}$ or $q''_{MHF} \le q''_{\text{film boiling}}\big\vert_{MHF}$, then film wetting regime does not exist. $q'' = q''_{MHF} + \frac{q''_{DFB} - q''_{MHF}}{(\Delta T_{DFB} - \Delta T_{MHF})^3}\left[(3\,\Delta T_{DFB} - \Delta T_{MHF})\,\Delta T_{MHF}^2 - 6\,\Delta T_{DFB}\,\Delta T_{MHF}\,\Delta T + 3\,(\Delta T_{DFB} + \Delta T_{MHF})\,\Delta T^2 - 2\,\Delta T^3\right]$ $+ \frac{\partial q''}{\partial \Delta T}\Big\vert_{DFB}\frac{1}{(\Delta T_{DFB} - \Delta T_{MHF})^2}\left[-\Delta T_{DFB}\,\Delta T_{MHF}^2 + (2\,\Delta T_{DFB} + \Delta T_{MHF})\,\Delta T_{MHF}\,\Delta T - (\Delta T_{DFB} + 2\,\Delta T_{MHF})\,\Delta T^2 + \Delta T^3\right]$ $\frac{\partial q''}{\partial \Delta T}\Big\vert_{DFB} = \frac{\partial q''_{\text{film boiling}}}{\partial \Delta T}\Big\vert_{DFB} = 107.0\,\Delta T_{DFB}^{0.691}\,Q''^{0.264}\,d_{32}^{-0.062}$ $= 1.164\times10^{4}\,Q''^{0.397}\,U_m^{0.0995}\,d_{32}^{-0.0366}$
Point of Minimum Heat Flux	$\Delta T_{MHF} = 204.9\,Q''^{0.066}\,U_m^{0.138}\,d_{32}^{-0.035}$ $q''_{MHF} = 3.324\times10^{6}\,Q''^{0.544}\,U_m^{0.324}$ If film wetting regime does not exist, then $q''_{MHF} = q''_{\text{film boiling}}\big\vert_{MHF} = 63.25\,\Delta T_{MHF}^{1.691}\,Q''^{0.264}\,d_{32}^{-0.062}$ $= 5.127\times10^{5}\,Q''^{0.376}\,U_m^{0.233}\,d_{32}^{-0.121}$
Transition Boiling Regime (Ref 16)	$q'' = q''_{CHF} - \frac{q''_{CHF} - q''_{MHF}}{(\Delta T_{CHF} - \Delta T_{MHF})^3}\left[(\Delta T_{CHF} - 3\,\Delta T_{MHF})\,\Delta T_{CHF}^2 + 6\,\Delta T_{CHF}\,\Delta T_{MHF}\,\Delta T - 3\,(\Delta T_{CHF} + \Delta T_{MHF})\,\Delta T^2 + 2\,\Delta T^3\right]$
Point of Critical Heat Flux (Ref 17)	$\Delta T_{CHF} = 18.0\left[(\rho_g\,h_{fg}\,Q'')\left(\frac{\sigma}{\rho_f\,Q''^2\,d_{32}}\right)^{0.198}\right]^{1/5.55}$ $\frac{q''_{CHF}}{\rho_g\,h_{fg}\,Q''} = 122.4\left[1 + 0.0118\left(\frac{\rho_g}{\rho_f}\right)^{1/4}\left(\frac{\rho_f\,c_{p,f}\,\Delta T_{sub}}{\rho_g\,h_{fg}}\right)\right]\left(\frac{\sigma}{\rho_f\,Q''^2\,d_{32}}\right)^{0.198}$
Nucleate Boiling Regime (Ref 17)	$q'' = 1.87\times10^{-5}\,(\Delta T)^{5.55}$
Onset of Single-Phase Cooling (Ref 17)	$\Delta T_{OSP} = 13.43\,Re_{32}^{0.167}\,Pr_f^{0.123}\left(\frac{k_f}{d_{32}}\right)^{0.220}$
Single-Phase Cooling Regime (Ref 17)	$Nu_{32} = 2.512\,Re_{32}^{0.76}\,Pr_f^{0.56}$

Units of the parameters: q'' [W m^{-2}], $\Delta T = T_s - T_f$ [°C], Q'' [m^3 s^{-1} m^{-2}], U_m [m s^{-1}], d_{32} [m], h [W m^{-2} K^{-1}], ρ_l [kg m^{-3}], ρ_g [kg m^{-3}], h_{fg} [J kg^{-1}], $c_{p,f}$ [J kg^{-1} K^{-1}], k_f [W m^{-1} K^{-1}], μ_l [N s m^{-2}], σ [N m^{-1}].
Dimensionless parameters: $Nu_{32} = h\,d_{32}/k_f$, $Pr_f = c_{p,f}\,\mu_f/k_f$, $Re_{32} = \rho_f\,Q''\,d_{32}/\mu_f$
Range of validity of the correlations:
$T_f = 23$ °C, $Q'' = 0.58\times10^{-3} - 9.96\times10^{-3}$ m^3 s^{-1} m^{-2}, $U_m = 10.1 - 29.9$ m s^{-1}, $d_{32} = 137\times10^{-6} - 1350\times10^{-6}$ m.
Properties: The fluid properties used in the correlations for the onset of single-phase cooling and the single-phase cooling regime are evaluated at the film temperature, $T_{film} = 0.5\,(T_s + T_l)$. The fluid properties used in the CHF correlations are evaluated at the fluid saturation temperature (Ref 17).

Obviously, the accuracy of the heat transfer boundary condition in a numerical analysis is of utmost importance. Figure 4 proves that the heat transfer correlations developed by the present authors, Klinzing et al. (Ref 16), and Mudawar and Valentine (Ref 17) accurately describe all of the boiling regimes experienced by a metallic part undergoing spray quenching. Furthermore, these correlations are universal to all spray types (full cone, hollow cone, and flat sprays) provided that the local spray hydrodynamic parameters are within the specified limits. The next section introduces a method for incorporating these correlations into boundary conditions for a numerical analysis which models the quenching of an alloy with multiple overlapping sprays.

4. Numerical Simulation of the Quenching Process

The numerical analysis of the spray quenching process involved solving the transient heat diffusion equation with temperature-dependent material properties (Ref 24) and temperature- and spatially-dependent boundary conditions. The ability of the commercial finite element program ABAQUS (Ref 25) to solve this problem with a user-defined nonuniform heat transfer coefficient made it ideal for the present study. Additional benefits included an efficient nonlinear equation solver and a self-adaptive time stepping scheme.

Since the ultimate objective of the present research is to numerically optimize the quenching process by changing nozzle configurations, surfaces of the part may or may not be in contact with a water spray. The ABAQUS input file (Ref 26) was generalized to permit a convection boundary condition for all surface elements. Furthermore, the locations of large spatial temperature gradients were unknown, so that a uniform two-dimensional finite element mesh was required. The input file contained a FORTRAN subroutine which defined the heat transfer coefficient as a function of surface temperature and surface location relative to the spray nozzles. The subroutine was consulted for each surface node at every iteration of every

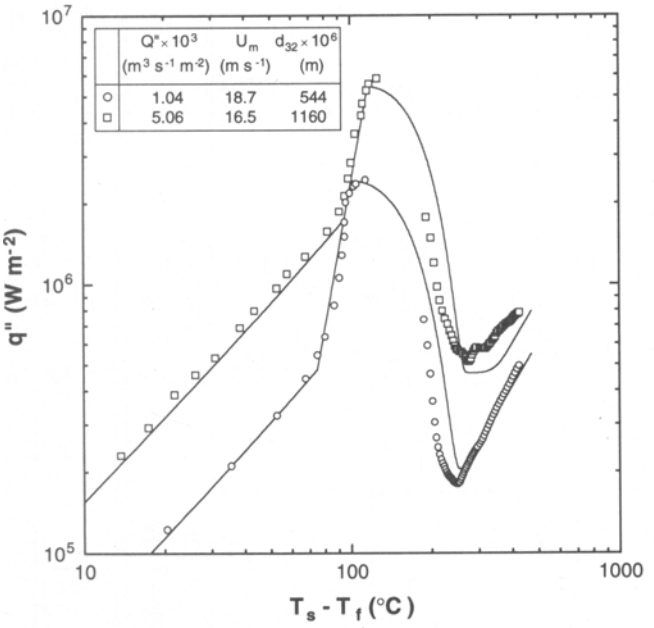

Fig. 4 Comparison of transient and steady-state spray heat transfer data with spray boiling curves calculated using the improved spray quenching heat transfer correlations

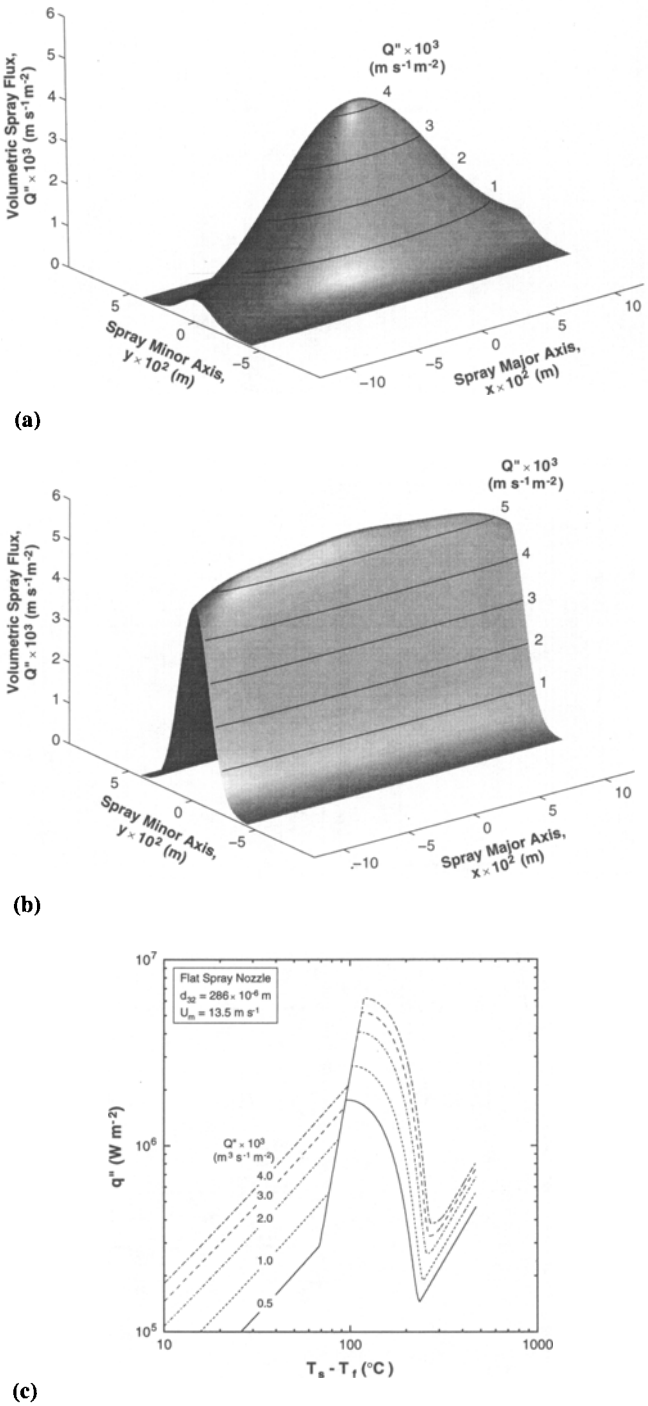

Fig. 5 Spatial distribution model of volumetric spray flux for (a) single flat spray nozzle and (b) optimized nozzle configuration, consisting of three flat spray nozzles separated by 11.4 cm (4.5 in.) along the spray major axis, utilized in the present study. (c) Calculated spray boiling curves for locations within the spray field corresponding to volumetric spray fluxes of 4.0×10^{-3}, 3.0×10^{-3}, 2.0×10^{-3}, 1.0×10^{-3}, and 0.5×10^{-3} $m^3\ s^{-1}\ m^{-2}$

time increment. The subroutine performed the following tasks if the location was being sprayed: (1) local spray hydrodynamic parameters were calculated; (2) the boiling regime experienced at this location was determined by comparing the current nodal temperature with the T_{DFB}, T_{MHF}, T_{CHF}, and T_{OSP} predicted using the correlations (see Fig. 3b); (3) local surface heat flux was calculated using the correlation corresponding to the boiling regime determined in step 2; and (4) the convection heat transfer coefficient was defined as $h = q''/\Delta T$. Radiation heat transfer from sprayed surfaces was neglected since the heat transfer coefficient due to radiation alone, based on a surface temperature of 495 °C and an emissivity of 0.15 (Ref 27), was less than 0.6% of the lowest value of the heat transfer coefficient due to spray convection (determined using the film boiling correlation listed in Table 2 for a location near the edge of a typical spray field). Natural convection and radiation from unsprayed surfaces were found to have a negligible effect on the numerical results. ABAQUS iterated each time increment until the solution at each node differed by less than 0.01 °C between iterations. A nearly continuous temperature-time history was obtained by defining a maximum allowable time increment of 0.1 sec. Solution convergence was investigated to determine the appropriate element type and size required by the present problem (1.25×1.25 mm^2 quadratic elements).

5. Experimental Validation of Spray Quenching Model

5.1 *Materials Processing Test Bed*

The Materials Processing Test Bed located at the Purdue University Boiling and Two-Phase Flow Laboratory was used to simulate the heat treatment process (solution heat treating, spray quenching, and artificial aging) of aluminum alloys in an industrial environment. Figure 6(a) shows a schematic containing the major components (furnace, translation system, spray chamber, quench tank, external plumbing, and data acquisition and processing system) of the facility. A vertical translation system lowered the testpiece from a tube furnace mounted above the quench tank into the spray chamber. Steam produced by the quench was removed by an exhaust system connected to the back of the test chamber. Water stored in the quench tank was circulated using a fan-cooled centrifugal pump, rated to deliver 25.2×10^{-3} m^3 s^{-1} (40 gpm) at 690 kPa (100 psi). A filter removed impurities from the water which could possibly accumulate near the nozzle orifice and cause flow blockage. The facility currently has a moveable nozzle array mounted on each side of the spray chamber, which allow flexibility of nozzle positioning relative to the testpiece. Each independently controlled nozzle array consisted of three nozzles vertically separated by 11.4 cm (4.5 in.) with the nozzle orifices 30.5 cm (12.0 in.) from the testpiece surface. Chromel-Alumel (type K) thermocouples were strategically located in a plane one-fourth the length of the testpiece above the lower surface. The testpiece surface was carefully polished to ensure uniform surface texture and repeatability between quenches. This treatment was required because surface roughness was observed to influence the thermal response of spray-quenched parts (Ref 28). Furthermore, the spray quenching heat transfer correlations used in the present numerical study were developed using polished surfaces (Ref 16, 17).

The heat treating schedule for an Al 2024-T6 extrusion having a maximum cross-sectional thickness of 31.8 mm (1.25 in.) and the desired evolution of the alloy microstructure are shown in Fig. 6(b). Testing commenced with the raising of the testpiece into the furnace using the vertical translation system. When the testpiece reached the solution heat treatment temperature, its temperature was constantly monitored to avoid overheating. The soaking time at the solution heat treatment temperature depends upon the type of product, alloy composition, fabrication procedure, and section thickness. ASM recommends a time of 70 min for a 12.7 mm (0.5 in.) thick wrought aluminum alloy when an air furnace is used (add 30 min for each additional 12.7 mm or fraction thereof in thickness). The quenching process was initiated by engaging the pump and allowing the sprays to reach hydrodynamic equilibrium. The testpiece was quickly lowered into the spray chamber using the translation system, and thermocouple output was recorded every 0.1 sec during the quench. The subsequent artificial aging process resulting in the T6 temper for extruded Al 2024 consisted of 16 hr at 190 °C. After heat treatment, a Goko Seiki Works model 3R hardness tester was used to measure Rockwell B hardness according to ASTM standard E 18 (Ref 29).

The L-shaped testpieces shown in Fig. 7 were machined from Al 2024 extrusions. The testpieces were designed so that the effects of section thickness and spray configuration on cooling uniformity could be investigated both experimentally and numerically. The L-shapes had a thermal mass ratio of 5:1 (Fig. 7a) or 4:1 (Fig. 7b) between the thick and thin sections. The L-shape in Fig. 7(a) was repeatedly quenched using different nozzle configurations, while the L-shape in Fig. 7(b) was subjected to a single heat treatment, in order to validate temperature and hardness predictions, respectively.

5.2 *Validation of Temperature Predictions*

The thermal history of an L-shaped extrusion quenched with multiple, partially overlapping sprays was predicted using the finite element method to solve the transient heat diffusion equation with temperature- and spatially-dependent boundary conditions. Spray quenching tests were conducted using the Materials Processing Test Bed with a nozzle array containing flat sprays impinging each side of the testpiece. Figure 8 compares predicted temperature-time curves with measurements obtained in a plane one-fourth of the entire testpiece length above the lower surface. The temperature-time history of the slowest-cooling (center of thick section) and fastest-cooling (surface of thin section near spray centerline) thermocouples were presented to demonstrate the ability to accurately predict the extreme cooling rates experienced within a quenched part. Overall, the predictions, including those not shown in Fig. 8, compare quite well with experiment. The most notable feature of the cooling curves is the sharp drop in temperature immediately following MHF. By predicting, and subsequently controlling, the occurrence of MHF, it may be possible to delay or advance the onset of the high cooling rates associated with the transition and nucleate boiling regimes such that the alloy cools more uniformly, resulting in improved mechanical and metal-

lurgical properties throughout the alloy. Experiments using different types of flat spray nozzles (Ref 18) and different nozzle configurations (Ref 26) were in similar agreement with numerical results, confirming that the method developed in the present study accurately predicts the thermal history of metallic parts subjected to spray quenching.

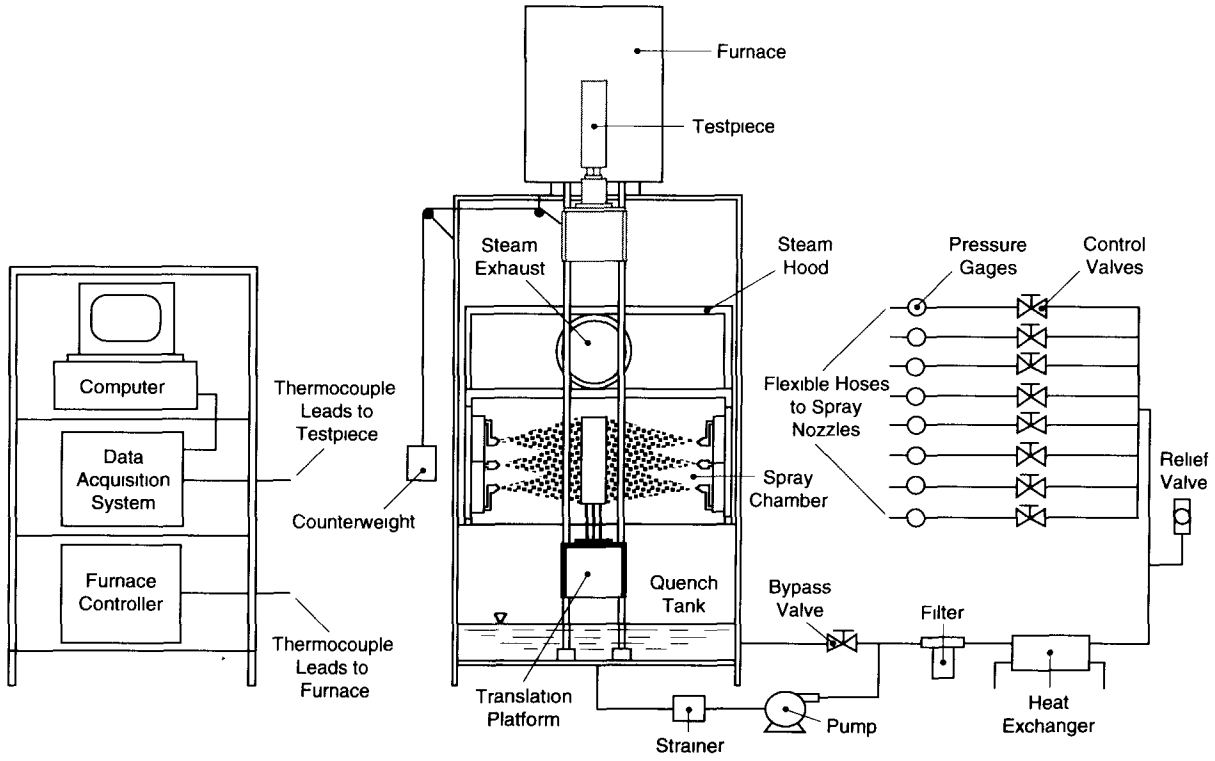

(a)

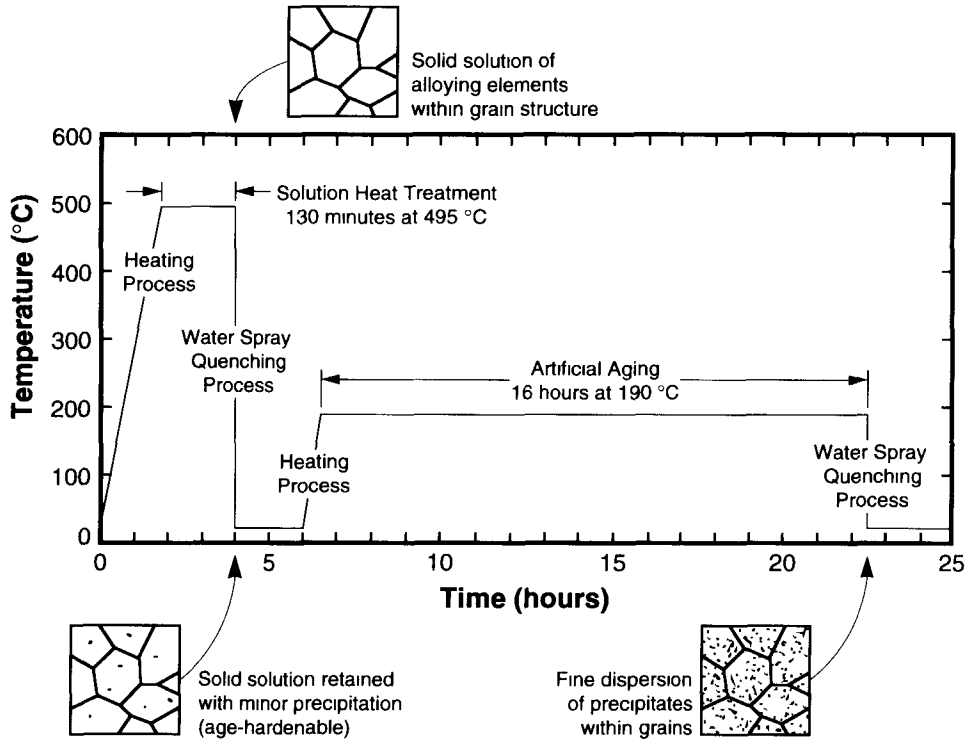

(b)

Fig. 6 (a) Schematic of the Materials Processing Test Bed and (b) heat treating schedule for an L-shaped Al 2024-T6 extrusion showing the desired evolution of the alloy microstructure

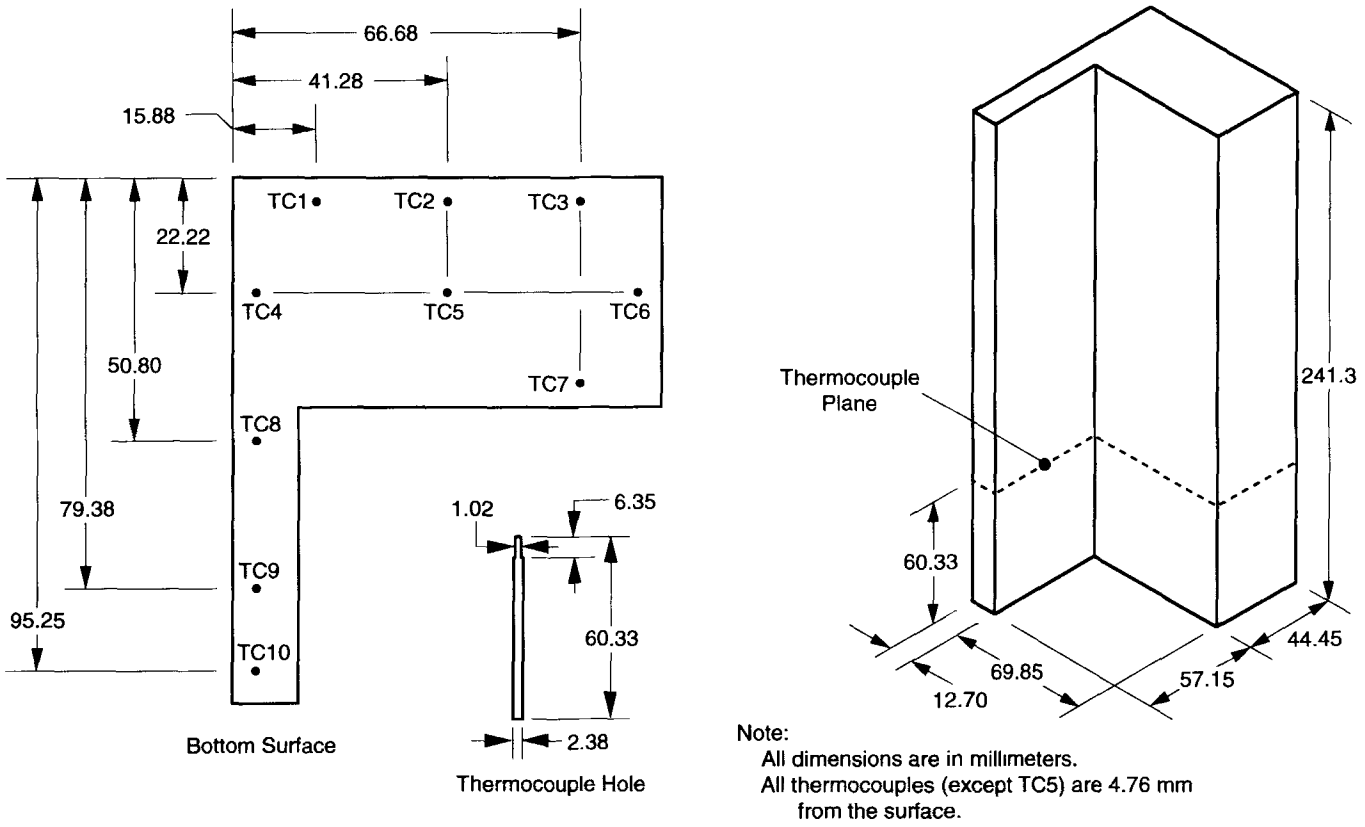

(a)

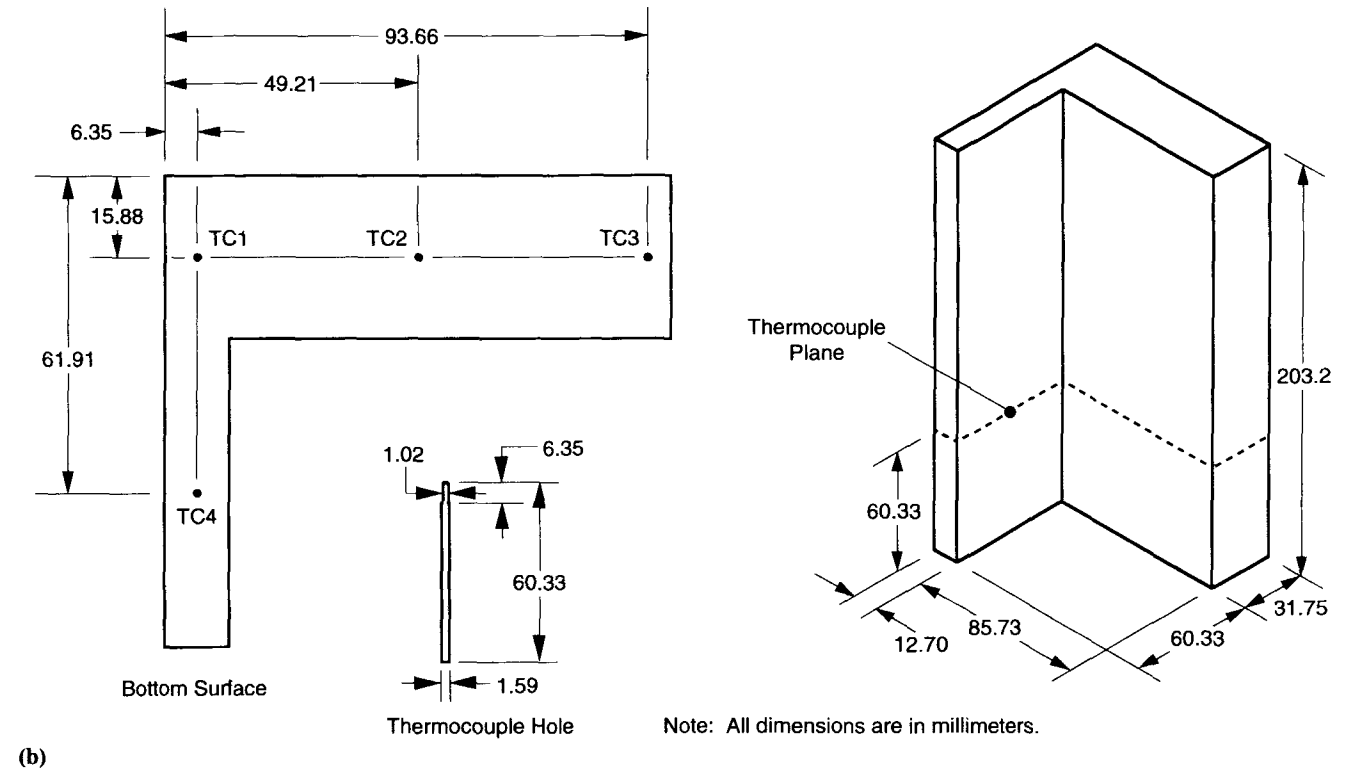

(b)

Fig. 7 Dimensions and thermocouple placement for the Al 2024 L-shaped extrusions used for validation of (a) temperature and (b) hardness predictions

5.3 *Validation of Rockwell Hardness Predictions*

The L-shaped extrusion shown in Fig. 7(b) was solution heat treated, spray quenched, and artificially aged to achieve the T6 temper. An alternate nozzle configuration was utilized during quenching so that axial uniformity and in-plane variations of hardness would be obtained in the heat-treated part. The in-plane variations of hardness were necessary to verify that the quench factor technique accurately predicts the trends in hardness throughout the part cross section. Previous experiments indicated that a single nozzle array (consisting of three optimally spaced nozzles whose major axes coincide) impinging the thin section yielded the largest possible variation of in-plane hardness using this type of nozzle and operating pressure (Ref 26). This realistic nozzle configuration was justified by viewing the L-shape as the symmetric fourth of an I-beam extrusion where the upper and rightmost surface of the L-shape are not cooled, since they represent adiabatic lines of symmetry. The web thickness of an I-beam is usually less than the flange thickness. However, the thicker web used in the present study was necessary to promote in-plane hardness variations.

Figure 9(a) shows Rockwell B hardness (HRB) measured on the exterior of a *nonuniformly* quenched L-shape and hardness contours predicted by coupling the quench factor technique with the predicted thermal history. The overall trends in hardness were accurately predicted throughout the L-shape, with the point of minimum predicted hardness and minimum measured hardness coinciding. Internal hardness measurements (not shown in Fig. 9a) obtained after sectioning the L-shape perpendicular to the extrusion direction also agreed with the predicted hardness trends. Additional measurements conducted on other planes parallel to the thermocouple plane confirmed the axial uniformity of hardness. The difference between measured and predicted hardness was a maximum in the thick section. This was attributed to significant forced convection from unsprayed surfaces of the testpiece to mist and air currents inside the spray chamber. The methodology developed in the current study accounted only for natural convection from unsprayed surfaces, so the thick section cooled more quickly and had a slightly higher hardness than predicted. This phenomenon did not affect the ability of the method to accurately predict trends in hardness. Furthermore, this error should decrease when a larger portion of the surface is being sprayed (i.e., as the quench is improved by adding sprays to the thick section).

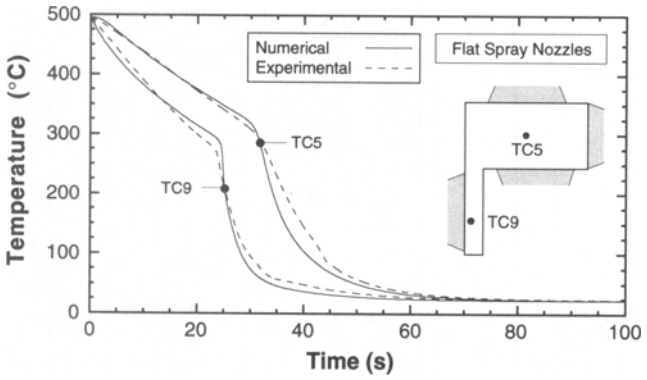

Fig. 8 Comparison of measured and predicted temperature-time curves of the L-shape during spray quenching

Figure 9(b) illustrates the predicted hardness contours of a *uniformly* quenched L-shape having the same dimensions and nozzle configuration as the L-shape utilized to validate the temperature predictions shown in Fig. 8. The uniform quench yielded hardness above 73 HRB and a variation of only 2.2 HRB throughout the L-shape. Although nearly a fourth of the nonuniformly quenched L-shape (Fig. 9a) was above 73 HRB, half of this L-shape was less than 66 HRB. Thus, a significant improvement in the magnitude and uniformity of hardness was obtained with uniform spray coverage for this particular cross section. Additional improvement of the uniform quench case is obtained by decreasing the thermal gradients, evidenced by the large temperature difference of the slowest- and fastest-cooling locations displayed in Fig. 8, while maintaining the high magnitude and uniformity of hardness. This can be accomplished by increasing the flow rate of the upper nozzle array and decreasing the flow rate of the left nozzle array so that the overall cooling rates of both sections become equivalent (Ref 31).

The maximum attainable hardness for Al 2024-T6, H_{max} in Eq 2, may be approximately 2 HRB higher than the value used to predict hardness in the present study (Ref 32). Thus, hardness predicted using the quench factor technique has an uncertainty of approximately 2.5%. This uncertainty, combined with the uncertainty associated with the calibration of the hardness tester, explains any differences in magnitude between measured and predicted hardness. Furthermore, these uncertainties do not affect the hardness trends (measured or predicted) observed within the L-shape. Since the quench factor technique has been validated for both strength and hardness in previous studies, the methodology developed in this study should also give accurate yield strength predictions.

6. Application of Spray Quenching Technology to Metal-Matrix Composites and Cast Alloys

Although metal-matrix composites (MMCs) have been active subjects of applied research for several decades, these composites have become realistic contenders as engineering materials only in the last few years. MMCs have emerged as candidates for advanced structural, aerospace, automotive, electronic, thermal management, and wear-resistant applications. They incorporate a wide variety of metal systems (e.g., Al, Mg, Ti, Cu, Fe, and Ni alloys) using several types of reinforcements (e.g., particulates, whiskers, and fibers). MMCs offer superior performance over conventional materials because of their tailorable physical, mechanical, and thermal properties, which include low density, high specific strength (high strength-to-weight ratio), high specific modulus (high ratio of elastic modulus to weight), elevated-temperature stability, high thermal conductivity, good fatigue response, control of thermal expansion, and high abrasion and wear resistance. The ability to combine different materials to control these properties makes composites attractive in many advanced engineering applications. However, several issues (interfacial bonding

between the reinforcement and matrix, residual stresses, matrix dislocations generated by the thermal mismatch between phases, and *reinforcement-induced alterations in matrix precipitation kinetics*) require a deeper understanding before MMCs gain widespread acceptance as reliable and affordable materials (Ref 33).

MMCs have been finding increasing use in electronic packaging, especially in avionics, where the higher costs can be justified by the weight savings. Electronic packaging materials are required to structurally support electronic components, provide protection from hostile environments, and dissipate excess heat generated by electronic components. This application requires high stiffness (i.e., high resistance to elastic strain), high thermal conductivity for heat dissipation, very low coefficient of thermal expansion, and low density while maintaining adequate strength (i.e., high specific strength), which are typical of a high volume-fraction, SiC_p-reinforced, aluminum-matrix (such as Al 6061) composite (Ref 34). Figure 10 is an example of an electronics enclosure, utilized in military avionics, which must be fabricated from a high-strength yet lightweight material such as a wrought, ceramic-reinforced, aluminum-matrix composite (Ref 35).

The addition of a brittle reinforcement to a precipitation-hardenable alloy can significantly alter the nucleation and growth kinetics of precipitation in the matrix as compared to those in the unreinforced monolithic alloy (Ref 36). Quenching from the solution heat treatment temperature generates thermal stresses due to the much lower coefficient of thermal expansion of SiC than that of the aluminum alloy. The matrix undergoes plastic deformation as the magnitude of local residual stresses exceeds the yield strength, promoting a higher dislocation density in the matrix of the composite (near SiC/Al interfaces) than in the unreinforced alloy. During artificial aging treatments, these dislocations (extra half-planes of atoms in an otherwise perfect crystal) serve as heterogeneous sites for the nucleation of strengthening precipitates and shorten the mean diffusion path for solute atoms. Accelerated aging occurs in the matrix since the nucleation and growth rates are larger than in the unreinforced alloy (Ref 37). The precipitates prevent plastic deformation of the crystal by prohibiting movement of dislocations (atomic planes sliding past each other) when the heat-treated composite is subjected to an external loading. The peak hardness or strength associated with a critical dispersion of precipitates occurs after a much shorter aging time than for the monolithic alloy, and caution must be observed to prevent overaging and subsequent loss in strength (Ref 38).

Macroscopic hardness measurements (such as Rockwell B or Brinell) include contributions from both the matrix (including that from precipitation) and the reinforcement. If a substantial hardening is directly caused by the reinforcement, then a macroscopic measurement, which still indicates the true hardness of the composite, may hinder the development of the matrix C-curve. In this case, microhardness measurements (such as Vickers) in regions of the matrix of the composite that have relatively few reinforcement particles may be required to develop the matrix C-curve which relates precipitation to matrix

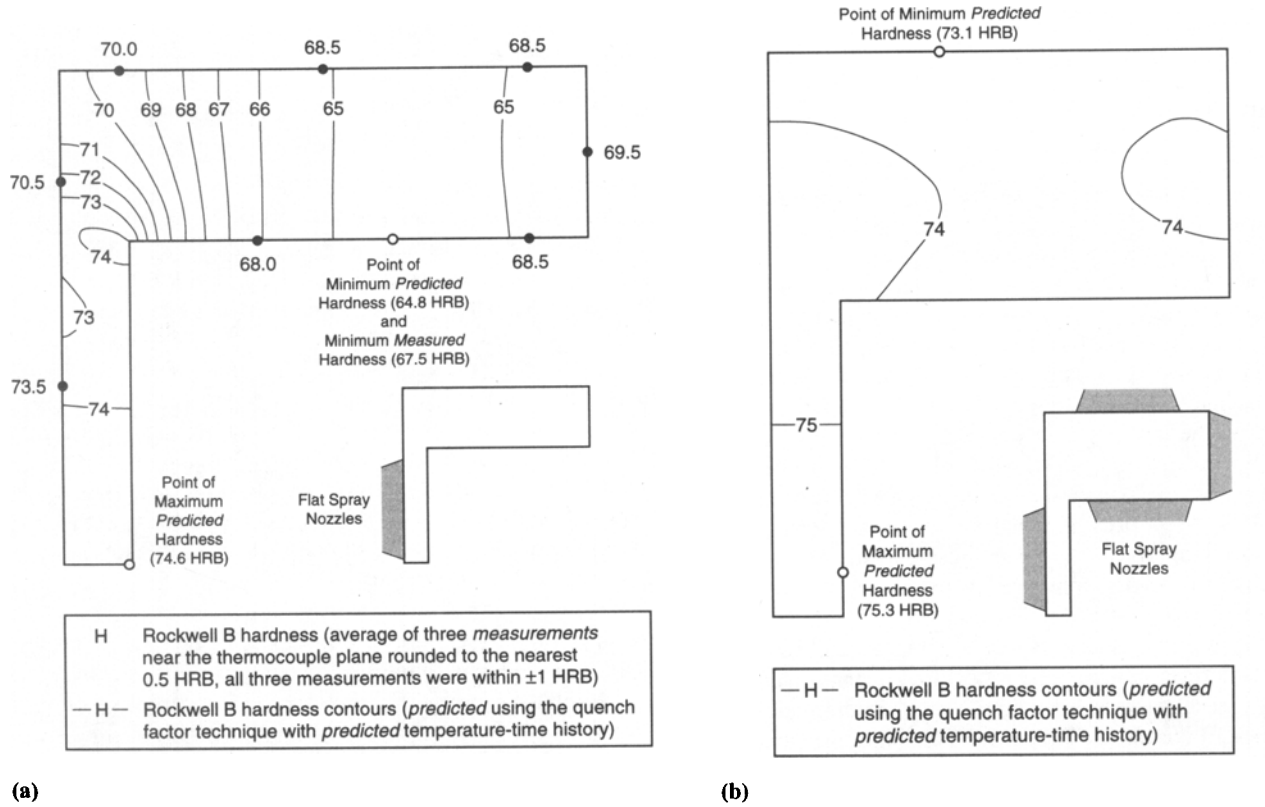

Fig. 9 Rockwell B hardness of a heat-treated L-shape resulting from (a) nonuniform and (b) uniform spray quenching. Source for Fig. 9(a): Ref 30

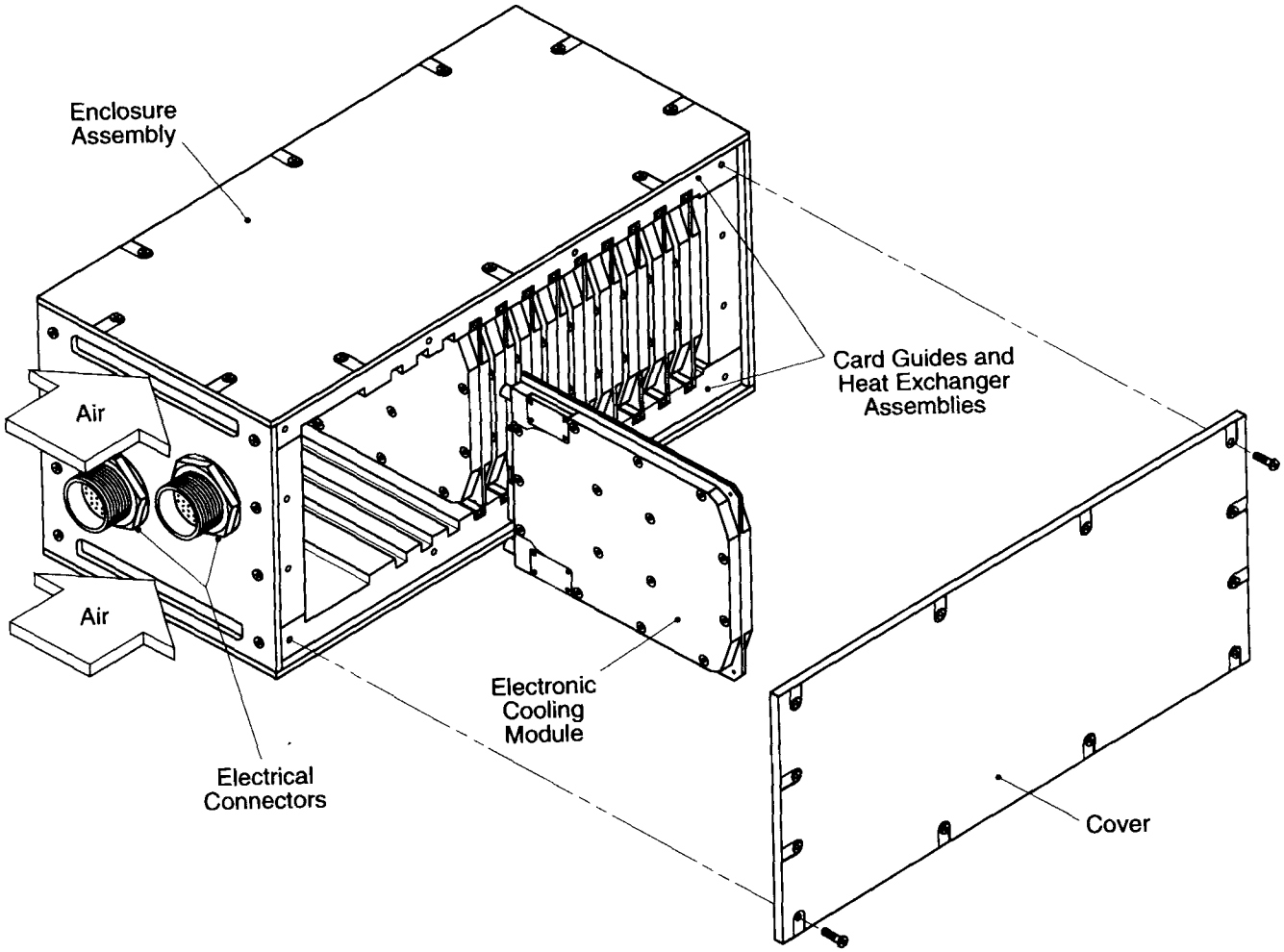

Fig. 10 A military avionics enclosure requiring a high specific strength material such as an aluminum matrix composite. Source: Ref 35

hardness. Several researchers have also found that precipitation during aging has a significant effect on ductility, ultimate tensile strength, fracture resistance, fatigue crack growth resistance, and corrosion and wear resistance, even when most strengthening is derived from the reinforcements (Ref 36). However, models based on the classical composite strengthening mechanism of load transfer (which ignores the higher dislocation density and accelerated aging) were incapable of explaining the increase in strength due to the addition of SiC particles or whiskers to an Al 1100, 6061, or 7091 matrix (Ref 39). Furthermore, Appendino et al. (Ref 38) and Niklas et al. (Ref 40) successfully employed macroscopic hardness measurements to document the differences between the precipitation kinetics of reinforced (10 to 20 vol% SiC_p) and unreinforced Al 6061.

Rapid, uniform quenching of a complex-shaped wrought MMC would further increase dislocation density while maintaining a near net-shape, leading to an even more substantial hardening of the MMC. The focus of an ongoing research program at the Aircraft Division of the Naval Air Warfare Center is the application of quench factor analysis to SiC_p/Al composites after extrusion into a near net-shape (Ref 41). Since the presence of the SiC_p reinforcement alters the precipitation kinetics of the age-hardenable Al 6061 matrix, the C-curve for the monolithic alloy cannot be utilized to predict the strength of the matrix. A delayed quenching technique (Ref 2) is being utilized to determine C-curves based on Rockwell B hardness for SiC_p/Al 6061 MMCs having various particulate volume fractions. Small-scale quenching experiments to confirm the applicability of quench factor analysis are anticipated in the near future, followed by large-scale experimentation using complex-shaped MMCs. Numerical modeling of the spray quenching process will be accomplished using the methodology developed at the Purdue University Boiling and Two-Phase Flow Laboratory. Improvement of the matrix strength through intelligent spray quenching should yield a significant increase in overall composite strength.

Recently, in an effort to substantially reduce costs and increase productivity, the aluminum industry has proposed casting irregularly shaped billets into a finished product, thus bypassing bulk deformation (e.g., extruding) or machining of a cylindrical billet. Thermal stresses occur during solidification, causing surface cracking or internal hot tearing defects which make the part unsuitable for commercial use. These stresses can be minimized by strategically locating and operating multiple spray nozzle arrays such that the

part solidifies uniformly, albeit not an easy task for a complex-shaped casting. The intelligent spray quenching system developed for heat treating extrusions is ideally suited for this application as well.

7. Summary

The spray quenching of a complex-shaped aluminum alloy extrusion with multiple, overlapping spray nozzles was successfully modeled using a systematic methodology which couples spray hydrodynamic models, a spray interaction model, spray heat transfer correlations, the finite element method, C-curve, and the quench factor technique. New spray heat transfer correlations for the high-temperature boiling regimes were formulated so that the entire set of correlations produced a smooth, continuous boiling curve for all possible combinations of the spray hydrodynamic parameters within the specified parameter ranges. The new correlations offer increased accuracy over previous correlations and substantially reduce the computation time of the finite element code. The validity of this unique approach was demonstrated by comparing model predictions with the temperature response (and hardness after aging) of an L-shaped extrusion quenched in a simulated industrial environment.

Researchers at the Purdue University Boiling and Two-Phase Flow Laboratory are continuing the development of a CAD/CAM system which would facilitate on-site control of the quenching process. Experiments have recently been performed in which the initial nozzle configuration was selected based on thermal mass distribution of the extrusion (Ref 31). Subsequent quenches were improved by increasing the cooling rate of the slowest-cooling regions of the extrusion (or decreasing the cooling rate of the fastest-cooling regions) such that the magnitude and uniformity of hardness (and yield strength) was maximized while maintaining relatively low spatial temperature gradients (i.e., low residual stress). The final system will optimally cool complex-shaped extrusions and castings by manipulating spray nozzle locations and intensity so that mechanical properties are optimized. The benefits expected from the implementation of this new technology include superior part quality, greatly increased productivity, virtual elimination of scrap, and elimination of costly trial-and-error heat treatment operations.

Acknowledgments

The authors appreciate the technical assistance of Jerry Hagers, Rudolf Schick, and Chris Schaffer of Spraying Systems Company. Financial support for the first author was provided in the form of the U.S. Department of Energy Predoctoral Integrated Manufacturing Fellowship.

References

1. T.A. Deiters and I. Mudawar, Optimization of Spray Quenching for Aluminum Extrusion, Forging, or Continuous Casting, *J. Heat Treat.*, Vol 7, 1989, p 9-18
2. W.L. Fink and L.A. Willey, Quenching of 75S Aluminum Alloy, *Trans. AIME*, Vol 175, 1948, p 414-427
3. J.S. Kim, R.C. Hoff, and D.R. Gaskell, A Quench Factor Analysis of the Influence of Water Spray Quenching on the Age-Hardenability of Aluminum Alloys, *Materials Processing in the Computer Age*, V.R. Voller, M.S. Stachowicz, and B.G. Thomas, Ed., Minerals, Metals, & Materials Society, 1991, p 203-221
4. J.W. Evancho and J.T. Staley, Kinetics of Precipitation in Aluminum Alloys during Continuous Cooling, *Metall. Trans.*, Vol 5, 1974, p 43-47
5. J.T. Staley, Quench Factor Analysis of Aluminum Alloys, *Mater. Sci. Technol.*, Vol 3, 1987, p 923-935
6. J.W. Cahn, Transformation Kinetics during Continuous Cooling, *Acta Metall.*, Vol 4, 1956, p 572-575
7. S.E. Axter, "Effects of Interrupted Quenches on the Properties of Aluminum," CM80-409, Society of Manufacturing Engineers, 1980
8. Heat Treating of Aluminum Alloys, *ASM Handbook*, Vol 4, ASM International, 1991, p 841-879
9. M. Conserva and P. Fiorini, Interpretation of Quench-Sensitivity in Al-Zn-Mg-Cu Alloys, *Metall. Trans.*, Vol 4, 1973, p 857-862
10. J.W. Evancho, "Effects of Quenching on Strength and Toughness of 6351 Extrusions," 13-73-HQ40, Alcoa Laboratories, Alcoa Center, PA, 1973
11. R.R. Sawtell, Effects of Quenching Path in Aluminum Alloy 7075, *Aluminium*, Vol 60, 1984, p 198-202
12. C.E. Bates, Selecting Quenchants to Maximize Tensile Properties and Minimize Distortion in Aluminum Parts, *J. Heat Treat.*, Vol 5, 1987, p 27-40
13. C.E. Bates and G.E. Totten, Procedure for Quenching Media Selection to Maximize Tensile Properties and Minimize Distortion in Aluminum Alloy Parts, *Heat Treat. Met.*, Vol 15, 1988, p 89-97
14. C.E. Bates, Predicting Properties and Minimizing Residual Stress in Quenched Steel Parts, *J. Heat Treat.*, Vol 6, 1988, p 27-45
15. C.E. Bates and G.E. Totten, Application of Quench Factor Analysis to Predict Hardness under Laboratory and Production Conditions, *Quenching and Distortion Control*, G.E. Totten, Ed., ASM International, 1992, p 33-39
16. W.P. Klinzing, J.C. Rozzi, and I. Mudawar, Film and Transition Boiling Correlations for Quenching of Hot Surfaces with Water Sprays, *J. Heat Treat.*, Vol 9, 1992, p 91-103
17. I. Mudawar and W.S. Valentine, Determination of the Local Quench Curve for Spray-Cooled Metallic Surfaces, *J. Heat Treat.*, Vol 7, 1989, p 107-121
18. D.D. Hall and I. Mudawar, Experimental and Numerical Study of Quenching Complex-Shaped Metallic Alloys with Multiple, Overlapping Sprays, *Int. J. Heat Mass Transfer*, Vol 38, 1995, p 1201-1216
19. T.A. Deiters and I. Mudawar, Prediction of the Temperature-Time Cooling Curves for Three-Dimensional Aluminum Products during Spray Quenching, *J. Heat Treat.*, Vol 8, 1990, p 81-91
20. I. Mudawar and T.A. Deiters, A Universal Approach to Predicting Temperature Response of Metallic Parts to Spray Quenching, *Int. J. Heat Mass Transfer*, Vol 37, 1994, p 347-362
21. K.F. Wang, S. Chandrasekar, and H.T.Y. Yang, An Efficient 2D Finite Element Procedure for the Quenching Analysis with Phase Change, *ASME J. Eng. Ind.*, Vol 115, 1993, p 124-138
22. N. Zabaras, S. Mukherjee, and W.R. Arthur, A Numerical and Experimental Study of Quenching of Circular Cylinders, *J. Therm. Stresses*, Vol 10, 1987, p 177-191
23. J.C. Rozzi, W.P. Klinzing, and I. Mudawar, Effects of Spray Configuration on the Uniformity of Cooling Rate and Hardness in the Quenching of Aluminum Parts with Nonuniform Shapes, *J. Mater. Eng. Perform.*, Vol 1, 1992, p 49-60
24. C.F. Lucks and H.W. Deem, *Thermal Properties of Thirteen Metals*, STP 227, American Society for Testing Materials, 1958, p 11
25. *ABAQUS User's Manual*, Ver. 4.8, Hibbitt, Karlsson and Sorensen, Inc., Providence, RI, 1989

26. D.D. Hall, "A Method of Predicting and Optimizing the Thermal History and Resulting Mechanical Properties of Aluminum Alloy Parts Subjected to Spray Quenching," M.S. thesis, Purdue University, 1993
27. G.G. Gubareff, J.E. Janssen, and R.H. Torborg, *Thermal Radiation Properties Survey*, 2nd ed., Honeywell Research Center, 1960
28. J.C. Rozzi, "Quenching of Aluminum Parts Having Irregular Geometries Using Multiple Water Sprays," M.S. thesis, Purdue University, 1991
29. ASTM Designation E 18, "Standard Test Methods for Rockwell Hardness and Rockwell Superficial Hardness of Metallic Materials," *1995 Annual Book of ASTM Standards,* Vol 03.01, American Society for Testing and Materials, 1995, p 115-128
30. D.D. Hall and I. Mudawar, Predicting the Impact of Quenching on Mechanical Properties of Complex-Shaped Aluminum Alloy Parts, *ASME J. Heat Transfer,* Vol 117, 1995, p 479-488
31. D.D. Hall and I. Mudawar, Optimization of Quench History of Aluminum Parts for Superior Mechanical Properties, *Int. J. Heat Mass Transfer,* Vol 39, 1996, p 81-95
32. J.S. Kim, "Prediction of the Influence of Water Spray Quenching on the Age-Hardenability of Aluminum Alloy 2024," M.S. thesis, Purdue University, 1989
33. S. Suresh, A. Mortensen, and A. Needleman, Preface, *Fundamentals of Metal Matrix Composites,* S. Suresh, A. Mortensen, and A. Needleman, Ed., Butterworth-Heinemann, 1993, p vii-viii
34. M.J. Koczak, S.C. Khatri, J.E. Allison, and M.G. Bader, Metal-Matrix Composites for Ground Vehicle, Aerospace, and Industrial Applications, *Fundamentals of Metal Matrix Composites,* S. Suresh, A. Mortensen, and A. Needleman, Ed., Butterworth-Heinemann, 1993
35. I. Mudawar, P.E. Jimenez, and R.E. Morgan, Immersion-Cooled Standard Electronic Clamshell Module: A Building Block for Future High-Flux Avionic Systems, *ASME J. Electron. Packag.,* Vol 116, 1994, p 116-125
36. S. Suresh and K.K. Chawla, Aging Characteristics of Reinforced Metals, *Fundamentals of Metal Matrix Composites,* S. Suresh, A. Mortensen, and A. Needleman, Ed., Butterworth-Heinemann, 1993
37. I. Dutta and D.L. Bourell, A Theoretical and Experimental Study of Aluminum Alloy 6061-SiC Metal Matrix Composite to Identify the Operative Mechanism for Accelerated Aging, *Mater. Sci. Eng.,* Vol A112, 1989, p 67-77
38. P. Appendino, C. Badini, F. Marino, and A. Tomasi, 6061 Aluminum Alloy-SiC Particulate Composite: A Comparison between Aging Behaviour in T4 and T6 Treatments, *Mater. Sci. Eng.,* Vol A135, 1991, p 275-279
39. R.J. Arsenault, Relationship between Strengthening Mechanisms and Fracture Toughness of Discontinuous SiC/Al Composites, *J. Compos. Technol. Res.,* Vol 10, 1988, p 140-145
40. A. Niklas, L. Froyen, L. Delaey, and L. Buekenhout, Comparative Evaluation of Extrusion and Hot Isostatic Pressing as Fabrication Techniques for Al-SiC Composites, *Mater. Sci. Eng.,* Vol A135, 1991, p 225-229
41. R.E. Morgan, S.L. Ehlers, and C.C. Myers, "Investigation of Heat Transfer Mechanisms and Metallurgical Transformations in Metal Matrix Composites to Predict Quench Factors," ILIR FY 95 Annual Report, Naval Air Warfare Center, Aircraft Division, Indianapolis, IN, Sept 1995